

STRUCTURAL AND MICROSTRUCTURAL CHARACTERIZATION OF Al_xTi_{3-x} TITANIUM - BASE ALUMINIUM ALLOYS

CARACTERIZACIÓN ESTRUCTURAL Y MICROSTRUCTURAL DE ALEACIONES DE ALUMINIO CON BASE DE TITANIO DEL TIPO Al_xTi_{3-x}

A. PENTÓN-MADRIGAL^{a†}, A. DOS SANTOS BRANCO^a, B. CONCEPCIÓN-ROSABAL^b, L.A.S. DE OLIVEIRA^c

a) Facultad de Física - IMRE, Universidad de La Habana, San Lazaro y L. C. Habana, CP 10400, Cuba; arbelio@fisica.uh.cu[†]

b) Instituto de Ciencia y Tecnología de Materiales - IMRE, Universidad de La Habana, San Lazaro y L. C. Habana, CP 10400

c) Núcleo Multidisciplinar de Pesquisas em Nanotecnologia, Campus Prof. Geraldo Cidade, Universidade Federal do Rio de Janeiro, Rodovia Washington Luiz, km 105. 25240-005, Duque de Caxias, RJ, Brazil

[†] corresponding author

Recibido 01/03/2021; Aceptado 17/06/2022

Se presenta la caracterización estructural y microestructural de aleaciones de aluminio - titanio (Al_xTi_{3-x} , $0.05 \leq x \leq 0.20$) por medio de la técnica de difracción de rayos-X (DRX). El análisis mostró la ocurrencia de una transición de fase orden – desorden en el rango de composición estudiado. La presencia de una fase minoritaria fcc en la matriz hcp de la aleación Al_xTi_{3-x} mostró evidencia de la presencia de defectos de apilado, cuya probabilidad de ocurrencia depende de la composición química y la distancia entre capas atómicas (parámetro de orden). El análisis microestructural usando los métodos de Warren-Averbach y Williamson-Hall mostró que unadiminución del contenido de Al, no solo disminuye la probabilidad de ocurrencia de defectos planares sino que propicia una disminución del tamaño promedio de cristalitas y aun aumento del valor medio de la microdeformación no uniforme en la aleación. Los defectos de deformación (α) predominan en este tipo de aleación.

The structural and microstructural characterization by means of X-ray diffraction (XRD) of the aluminum-titanium alloys (Al_xTi_{3-x} , $0.05 \leq x \leq 0.20$) is presented. The analysis showed the occurrence of an order-disorder phase transition in the studied compositional range. The presence of a minor fcc phase within the hcp matrix of the Al_xTi_{3-x} alloy showed evidence of the presence of stacking faults. The probability of occurrence of this type of defect depends on the chemical composition and on the distance between atomic layers (order parameter). The microstructural analysis using the Warren-Averbach and Williamson-Hall methods shows that a decrease of Al content not only decreases the probability of occurrence of planar defects but also leads to a decrease in the average crystallite size and to an increase of the average non uniform microstrain value in the alloy. Deformation defects (α) predominate in this type of alloy.

PACS: Keywords. Crystal structure alloys (Estructura cristalina de aleaciones), 61.66.Dk; X-ray diffraction (Difracción de rayos X), 61.05.cp; microstructure (Microestructura), 61.72.-y; Crystal defects (Defectos cristalinos), 61.72.-y

I. INTRODUCTION

Aluminum – Titanium (AlTi) alloys have been continuously studied for many years due to their high impact in the industry. Mechanical alloying processes, doping with other elements, microstructure modification through assisted techniques, and other processes have provided ways to modify properties such as hardness, resistance to high temperatures, oxidation, corrosion, binding properties, etc. of Ti-base Al alloys [1–8]. All the reported studies have as a common feature: the structural and microstructural characterization of the alloys using, as fundamental techniques, X-ray diffraction (XRD) and electron microscopy.

The microstructure of these materials is determined by a complex distribution of structural defects, where planar defects (stacking faults) play an important role in the physical and mechanical properties of AlTi alloys. The quantitative determination of the probability of occurrence of this type of defect by different techniques and methods has been the object of study in a significant number of contributions [1], [5–8].

Reports on microstructural analysis in the Al_xTi_{3-x} system [6–8] show that the used procedure differs from the methodology

proposed in the Warren-Averbach (WA) method [9]. Instead of choosing reflections of different orders to separate the Fourier coefficients representing coherent domain size and microstrains, reflections not affected by planar defects are selected to determine both coefficients, even though the selected reflections are not perpendicular to the same crystal column (same crystallographic direction). In the cited references, reflections affected by planar defects are then used to determine the coefficients of what is usually called the effective coherent domain size, that is, the one that also taken into account the effect of this type of defect. This last group of reflections is not perpendicular to the same crystal column either, as the WA method requires.

The referred procedure can lead to incorrect results in the determination of the probabilities of occurrence of planar defects and, ultimately, uncertainties in the determination of coherent domain sizes and microstrains in the crystal structure of the alloy.

The analysis presented in this work is framed following the ideas of the WA method, at least in those cases where it is possible. An alternative method (Williamson - Hall) [10] is applied for the case where reflections of different orders are

not available. Additionally, a compositional phase transition in the studied composition range is qualitatively analyzed.

II. EXPERIMENTAL AND METHODS

II.1. Experimental procedure

Nominal $\text{Al}_x\text{Ti}_{3-x}$ compositions with, $0.05 \leq x \leq 0.20$ in the Ti-rich region of the Al-Ti binary phase diagram were prepared [11, 12]. The starting elements were high purity Al and Ti powders (99.9%). The alloy ingots were prepared by a standard arc melting method. The ingots were hot extruded at 800°C for 48 h to ensure homogeneity and then air-cooled. Part of the samples were reduced to powder, sieved to particles size less than $1 \mu\text{m}$ and subjected to a heat treatment at 100°C to reduce stresses.

The powder XRD patterns were recorded at room temperature in an X-Pert Panalytical diffractometer in a range $2\theta = 15^\circ - 90^\circ$ with a step of 0.02° in Bragg – Brentano configuration. The radiation used was $\text{Cu-K}_{\alpha 1}\text{-K}_{\alpha 2}$, at 35 kV and 20 mA. A standard sample of LaB_6 was also measured under the same conditions to account for instrument contributions to peak width.

The chemical composition of the samples was verified using X-ray energy dispersive spectroscopy (EDS) analysis in a TESCAN VEGA 3 LMU BME with an OXFORD X-MaxN 20 mm^2 detector coupled to the SEM.

II.2. Method of analysis

The diffraction maxima can be expressed through the Fourier series, whose coefficients are related to the microstructural characteristics of the material, i.e. coherent domain size, non-uniform microstrains, stacking faults, etc. [9]. The Fourier analysis is sensitive to statistical errors of the experimental data [13], so the analysis is more stable using certain analytical functions that properly describe the profile of the diffraction maximum [14].

The Fourier expansion coefficients (A_L) can be expressed, in turn, as the product of two terms resulting from the fundamental theorem of convolution of functions [15]:

$$A_L = A_L^S \cdot A_L^D \quad (1)$$

where A_L^S are coefficients depending on the crystal column length (L) perpendicular to the planes in diffraction conditions and they are called coherence length coefficients. The term A_L^D depends on the non-uniform microstrain of the crystal structure along with L and they are called microstrain coefficients.

The relation 1 provides the basis for using Fourier series analysis for the quantitative characterization of crystalline imperfections in randomly oriented polycrystalline samples.

2.2.1. Warren – Averbach method (WA)

The WA method is based on 1 and it proposes a formalism to separate both contributions mentioned above. According

to [9], the Fourier coefficients of a diffraction maximum can be expressed as:

$$\ln A_L = \ln A_L^S - 2\pi^2 l^2 \langle \epsilon_L^2 \rangle, \quad (2)$$

where the second term of 2 expresses the average value of the microstrain along the column L , while the variable l depends on the unit cell parameter along the crystallographic direction being considered.

Expression 2 states that if multiple order reflections can be measured for a given sample, then the Fourier expansion coefficients can be extracted. From $\ln A_L$ as a function of l^2 for a given set of harmonics, the A_L^S coefficients can be calculated from the intercepts, while the A_L^D coefficients are calculated from the microstrain values, which are determined by the slopes of 2.

The A_L^D values are calculated from the mean value of the microstrain considering a Gaussian or Cauchy type distribution [16, 17]. In the present work, a Cauchy type distribution 3 was considered, since it presents a much smoother fall in the diffraction profiles as observed in the experiments.

$$A_L^D = \exp\left(-\frac{\pi^2 L}{Cd} \langle \epsilon_L^2 \rangle\right),$$

where d is the interplanar distance of the peak, $\langle \epsilon_L^2 \rangle$ is the mean square displacement and C is called the “cut-off” point [17].

It is known that planar defects can be classified as coherent domain type defects. This means that when referring to the average effective coherent domain size ($\langle D_{eff} \rangle$), the effects of both average crystallite size and planar defects (along the same crystallographic direction) are taken into account. In order to separate the two contributions, reflections that meet the condition of being affected by this type of defect must be used: $h - k \neq 3n$, $n \in \mathbb{Z}$ together with those that do not meet the previous condition, where h and k are Miller indices. For diffraction maxima fulfilling the last condition, following relations hold [15]:

$$-\left(\frac{dA_L^S}{dL}\right)_{L \rightarrow 0} = \frac{1}{\langle D_{eff} \rangle} = \frac{1}{\langle D \rangle} + \left(|l| \frac{d}{c^2}\right) (3\alpha + 3\beta), \quad (3)$$

for $h - k \neq 3n$, with l even.

$$-\left(\frac{dA_L^S}{dL}\right)_{L \rightarrow 0} = \frac{1}{\langle D_{eff} \rangle} = \frac{1}{\langle D \rangle} + \left(|l| \frac{d}{c^2}\right) (3\alpha + \beta), \quad (4)$$

for $h - k \neq 3n$, with l odd.

While for those peaks that do not meet it, it holds:

$$-\left(\frac{dA_L^S}{dL}\right)_{L \rightarrow 0} = \frac{1}{\langle D \rangle}, \quad (5)$$

where $\langle D \rangle$ is the average value of crystallite size, while the left-hand side of 4 and 5 can be interpreted as an average effective coherent domain size ($\langle D_{eff} \rangle$).

Planar defects are determined from their probability of occurrence, α (deformation defect) and β (twin or growth).

In equations 3-5 the left-hand side is the first derivative of the initial A_L^S vs L curve. This result indicates that the intercept of the tangent to the curve at $L \rightarrow 0$ with the abscissa axis returns the value of $\langle D_{eff} \rangle$ from 3 and 4 and $\langle D \rangle$ from 5.

To implement the WA method, the free software WinFit [18] was used. The fitting of the diffraction maxima was carried out with the Pearson VII analytical function [19].

II.3. Williamson – Hall (WH) method

The WH method [10] expresses that the integral width of a diffraction maximum (β^* in reciprocal units) can be expressed as a linear combination of two terms:

$$\beta^* = \frac{1}{\langle D \rangle} + \frac{\eta}{2} d^* \quad (6)$$

where the inverse of the intercept with the ordinate returns the average coherent domain size $\langle D \rangle$, while the slope of 7 gives average non-uniform microstrain values. The use of this method in the present work does not take into account other microstructural effects that may result in the nonlinearity of 7.

III. RESULTS AND DISCUSSION

III.1. Analysis by Scanning Electron Microscopy

Table 1 shows the chemical composition determined by EDS. The chemical microanalysis confirms that samples have a composition close to the nominal one. Based on the AlTi alloy phase diagram [11, 12], the composition range is found in the Ti-rich zone where an order-disorder compositional phase transition occurs.

Table 1. Nominal and EDS-determined values of the alloy Al_xTi_{3-x} .

x nominal	x by EDS	AlTi %
0.05	0.04(5)	Al:4.5 % Ti:95.5 %
0.07	0.06(6)	Al:6.6 % Ti:93.4 %
0.15	0.14(5)	Al:14.5 % Ti:85.5 %
0.20	0.17(8)	Al:17.8 % Ti:82.2 %

III.2. Structural analysis

Fig 1 shows the XRD patterns of the studied alloys. The alloy crystallizes in a hexagonal close-packed crystal structure (hcp), with space group (SG): P63/mmc (ICSD 58188) [20]. A qualitative analysis shows that the (100), (101) and (110) reflections disappear with decreasing Al content. For the sample $x = 0.07$, the very low intensity (101) reflection can still be observed, but disappears completely for $x = 0.05$. This behavior suggests a phase transition, which will be explained later. The indexing is in correspondence with the main phases present in the samples and only the (hkl) of the most intense peaks have been indicated.

The occurrence of other low intensity reflections is observed for $x = 0.15$ y 0.20 (marked with arrows), which have been indexed as an AlTi fcc cubic phase with SG: Fm-3m (ICSD

43423) [20]. The most significant reflections, i.e. for $x = 0.20$, are: (111) at $2\theta = 36.41^\circ$ and (200) at $2\theta = 42.29^\circ$.

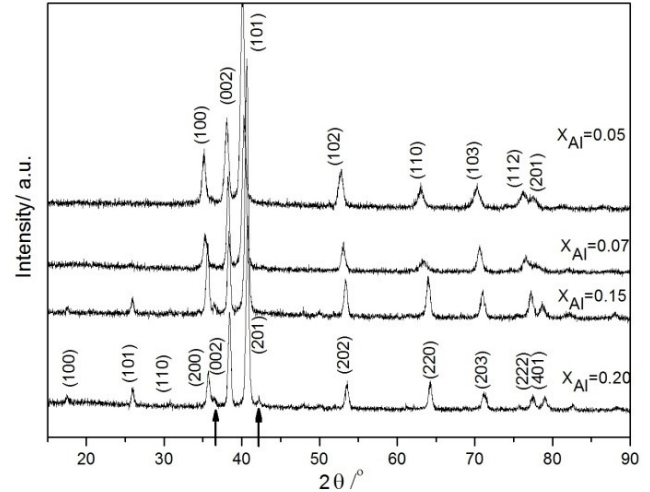


Figure 1. XRD patterns for Al_xTi_{3-x} with $0.05 \leq x \leq 0.20$.

The evolution of the lattice parameters, as well as the interplanar distance along the [001] direction, are shown in Table 2. The lattice parameter a shows a more significant change, while the parameter c increases slightly with decreasing Al content. The variation of the lattice parameters follows Vergas' law [21] describing a compositional order-disorder phase transition, typical of this type of solid solution. This transition is also responsible for the observed behavior of the (100), (101) and (110) reflections.

Table 2. Values of the lattice parameters for each composition, as well as the distance between atomic layers (d) along the [001] direction.

x nominal	a / Å	c / Å	d $c/2/\text{Å}$
0.05	2.94(4)	4.71(8)	2.35(9)
0.07	5.81(3) / 2.93(1)	4.69(0) / 4.69(1)	2.34(6) / 2.34(5)
0.15	5.80(8)	4.68(2)	2.34(1)
0.20	5.78(7)	4.66(9)	2.33(4)

Figure 2 shows the XRD patterns for $x = 0.05$, 0.07 and 0.20 in the same 2θ range. A detailed analysis reveals that with decreasing Al content the (200) reflection, for $x = 0.20$, splits into two not well-resolved reflections for $x = 0.07$, and then, a single reflection emerges again for $x = 0.05$. This effect is not observed for the (002) reflection. This behavior suggests a compositional phase change mainly affecting the basal plane of the hcp structure, which in turn results in an indexing change of the pattern.

The substitution of Al and Ti elements in the crystal structure can occur in an ordered or disordered manner. The compositional order-disorder transition occurs around $x = 0.07$.

This phase transition is represented in the phase diagram as $AlTi_3 \rightarrow \alpha\text{-Ti}$. For compositions $x = 0.20$, 0.15, substitutions occur in an ordered manner (Fig.3a), where Al occupies the $2c$ position and Ti the $6h$ position of the crystal structure described by the SG P63/mmc (No. 194) [22]. For $x = 0.07$, the

coexistence of both phases ($\text{AlTi}_3 + \alpha\text{-Ti}$) is evidenced. Finally, for $x = 0.05$, the system presents a completely disordered substitution ($\alpha\text{-Ti}$) in both crystallographic sites (Fig. 3b). In this situation, the new unit cell can be described by 1/4 of the cell of the ordered phase (Fig. 3c). It explains the transition observed for the unit cell parameter a (Table 2), as well as the absence of the (100), (101) and (110) reflections for $x = 0.05$, resulting in new indexing of the diffraction pattern once redefined the new crystallographic basis.

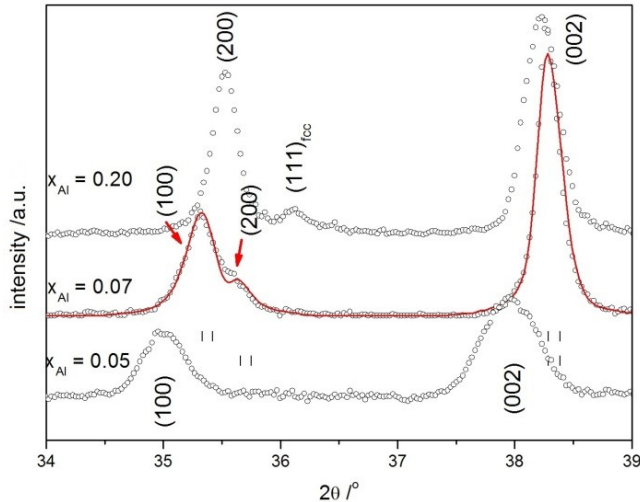


Figure 2. 2θ range for $x = 0.05$, 0.07 and 0.20 exhibiting a compositional order-disorder phase transition. Experimental data is represented with black circles, the calculated pattern with red solid line and calculated Bragg positions with vertical lines.

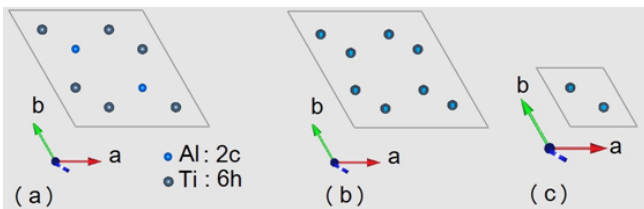


Figure 3. Basal plane projection of the ordered structure, (b) structure with random substitution and (c) new crystallographic basis describing the disordered system.

To confirm this crystallographic analysis, a diffraction pattern has been calculated from a structural model taking into account the occurrence of the ordered and disordered phases. The calculated pattern appears in Fig. 2 represented by the solid red curve superimposed on the experimental pattern (black circles) for $x = 0.07$, while the vertical bars at the bottom of the maxima correspond to the calculated Bragg positions for both phases. The calculated diffraction pattern supports the explanation given for the compositional phase transition from the crystallographic point of view. The intensities ratio of the (100) and (200) reflections for $x = 0.07$ suggests that the highest volume fraction corresponds to the disordered phase.

The increase of c with decreasing Al content (Table 2) may influence the type of stacking sequence dominant in the crystal structure. The interplanar distance is an order parameter determining the energy stability of a specific stacking sequence [23]. Large planar defects density in an hcp structure favors long-range stacking disorder in the crystal structure, which in turn results in the occurrence of observable

diffraction maxima associated with an fcc stacking sequence (arrows in Fig. 1). The increase of the interplanar distance, as a result of decreasing Al content, has a direct effect on the planar defects density, favoring the hcp sequence instead of the fcc one. It explains why (111) and (200) diffraction maxima of the fcc phase vanish as a function of Al content. This qualitative analysis will be confirmed once the quantitative analysis of the diffraction patterns is carried out in the next section.

IV. MICROSTRUCTURAL ANALYSIS

IV.1. Microstructural analysis for samples $x = 0.20 - 0.15$

The possibility of having (hkl) reflections of different orders, such as the pairs (100)/(200) and (101)/(202), allows a microstructural analysis approach within the framework of the WA method. For the analysis, the pair of reflections (101)/(202) was chosen on the basis of being reflections of different orders and affected by planar defects.

Figure 4 shows the calculation of the Fourier coefficients (A_L^S) from (101)/(202) for $x = 0.20$, 0.15 once the instrumental contribution has been removed. The intercept of the initial slope of each curve with the abscissa returns the average effective coherent domain size values $\langle D_{eff} \rangle = (21.7 \pm 0.5)$ nm and $\langle D_{eff} \rangle = (26.6 \pm 0.5)$ nm for $x = 0.20$ and $x = 0.15$, respectively.

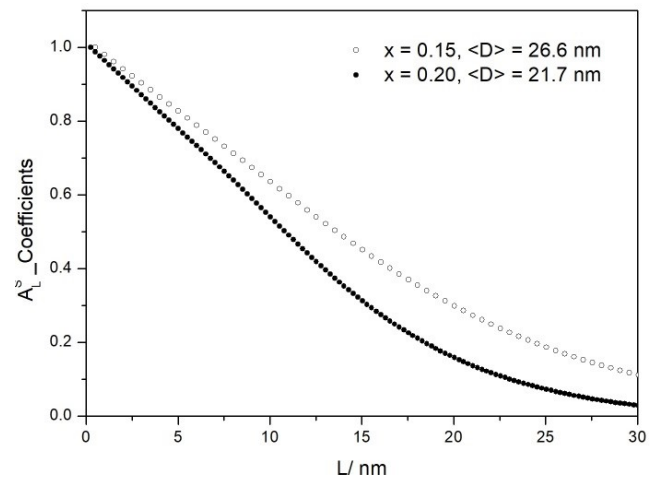


Figure 4. Fourier coefficients (A_L^S) from (101)/(202) for $x = 0.20$ and 0.15 .

The average non-uniform microstrain values calculated from the slopes of 3 for $x = 0.20$ y 0.15 were $\langle \epsilon \rangle = (1.0 \mp 0.4 \times 10^{-2}) \times 10^{-3}$ and $\langle \epsilon \rangle = (0.9 \mp 0.4 \times 10^{-2}) \times 10^{-3}$, respectively.

To determine the planar defects density, the 2θ range $50^\circ - 75^\circ$, i.e. for $x = 0.20$ is analyzed (Fig. 5). The procedure is the same for the sample $x = 0.15$. Two reflections hold the condition: $h - k \neq 3n$, $n \in \mathbb{Z}$ (peaks (202) and (203)), and one meets: $h - k = 3n$, $n \in \mathbb{Z}$, (220). It should also be noted that reflections affected by planar defects have an even and odd l index. This would allow these three peaks to be used to determine α and β defects probabilities using 3-5. But, to apply this methodology, higher-order (220) and (203) reflections are not available. This

limitation does not allow directly extracting the coefficients A_L^S and A_L^D from the Fourier coefficients $A_L^{(220)}$ and $A_L^{(203)}$.

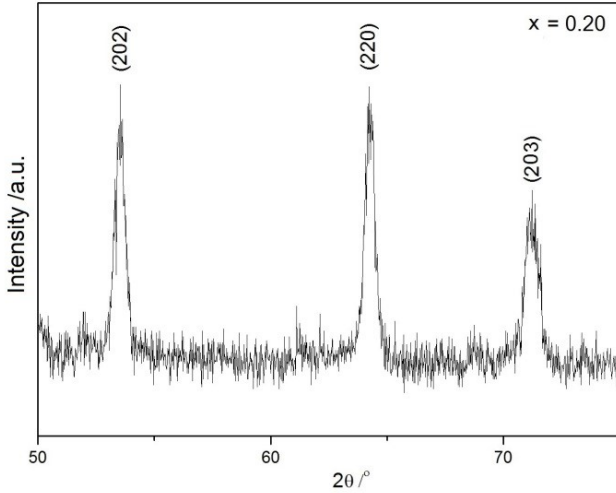


Figure 5. Fraction of the XRD pattern for $x=0.20$ showing reflections that satisfy the conditions $h-k \neq 3n$ and $h-k = 3n$, $n \in \mathbb{Z}$.

To overcome this difficulty, it will be assumed that microstrain coefficients (A_L^D) of (220) and (203) reflections can be described through the microstrain coefficients of the (202) reflection ($A_L^D_{(202)}$). Although these coefficients depend on the variable l , this approximation is made on the basis that the three diffraction maxima are not very far away angularly and that the microstrain distribution is isotropic.

The $A_L^D_{(202)}$ coefficients can be determined according to (3) using the known values of A_L and A_L^S for the (202) reflection. The procedure consists in fitting A_L coefficients by means of:

$$A_L = A_L^S \cdot \exp\left(-\frac{\pi^2 L}{Cd} \langle \epsilon_L^2 \rangle\right), \quad (7)$$

where C is the fitting parameter. Taking this approximation into account, the coherent domain size coefficients $A_L^S_{(220)}$ and $A_L^S_{(203)}$ can be determined through:

$$A_L^S_{(220)} = \frac{A_L^{(220)}}{A_L^D_{(202)}} \quad (8)$$

$$A_L^S_{(203)} = \frac{A_L^{(203)}}{A_L^D_{(202)}}.$$

From the curves of $A_L^S_{(220)}$ and $A_L^S_{(203)}$ vs L , the values of $\langle D \rangle$ and $\langle D_{eff} \rangle$ can be determined respectively, as shown in Table 3. Finally, using 3-5 the values of α and β are determined.

Table 3. $\langle D_{eff} \rangle$, $\langle D \rangle$ values, and deformation faults probability (α) for $x = 0.20, 0.15$.

x nominal	$\langle D_{eff} \rangle$ / nm	$\langle D \rangle$ / nm	$\langle D_{eff} \rangle$ / nm	$\alpha \times 10^{-3}$
0.20	21.7 ± 0.5	23.1 ± 0.5	13.3 ± 0.5	8.4 ± 0.4
0.15	26.6 ± 0.5	42.5 ± 0.5	18.8 ± 0.5	6.7 ± 0.4

The α values are of the same order as those reported in previous studies for this type of alloy, although the WA method in these reports is not based on the use of

different order reflections as previously mentioned [6–8]. The differences between the calculated values in similar compositions are probably due to the methodology used in each case, without ruling out an eventual experimental error in determining the integral width of the diffraction maxima. It is also reported that α defects predominate in this type of AlTi alloy decreasing its density with decreasing Al content.

The behavior of α as a function of the Al content supports the qualitative explanation made before regarding the occurrence of low-intensity reflections indexed as (111) and (200), typical of an fcc sequence within an hcp matrix and how they disappear for low Al concentrations (Fig. 1).

Finally, it is also reported by other authors [1, 6–8], that in this type of alloy the probabilities of occurrence of twinning (β) are negligible or return negative values, as in the present study. This result is interpreted as an absence of this type of defect in alloys with hcp-type structures.

IV.2. Microstructural analysis for $x = 0.05$

A qualitative analysis of the diffraction pattern for this composition shows that the behavior of the integral width values of the maxima as a function of 2θ can be described according to the Caglioti formula [24]. This behavior, known as isotropic type, suggests the non-presence, or non-detection, of planar defects in the crystal structure. It can then be assumed that the microstructure would be determined only by the average crystallite size and by the average non-uniform microstrains. Additionally, the indexing of the diffraction maxima using the redefined crystallographic base (Fig. 3c) causes multiple order reflections to not appear in the measurement range (Fig. 1).

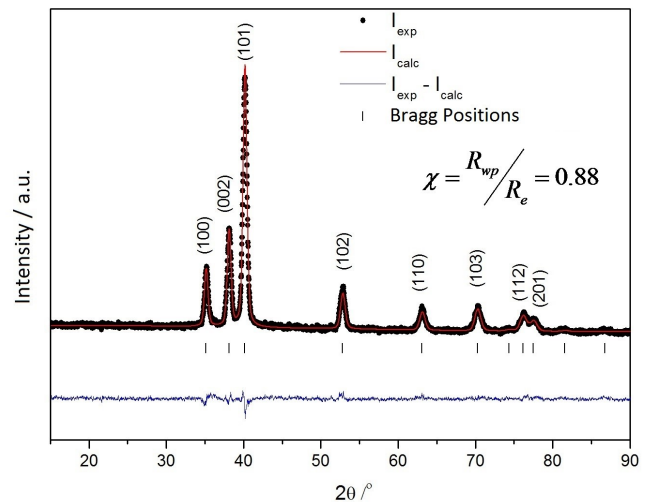


Figure 6. Result of the Rietveld refinement. Experimental pattern (dots), calculated pattern (red solid line), difference (blue curve below), calculated Bragg positions (vertical bars). Goodness of fit parameter $\chi = 0.88$.

To carry out the microstructure analysis of this sample, the WH method was used as an alternative way. For this study, the free software FullProf [25] based on the Rietveld method [26] in profile matching mode (Le Bail [27]) was implemented. A standard sample of LaB6 was also used to remove the instrumental contribution to the peaks.

Afterwards, the Rietveld refinement (Fig. 6), parameters describing peak profiles were determined. The integral width (β^*), according to (6), will be determined by the average coherent domain size ($\langle D \rangle$) and by nonuniform microstrains. In Fig. 7, the inverse of the intercept of the straight line with the ordinate returns $\langle D \rangle$, while the slope gives the average non-uniform microstrains value.

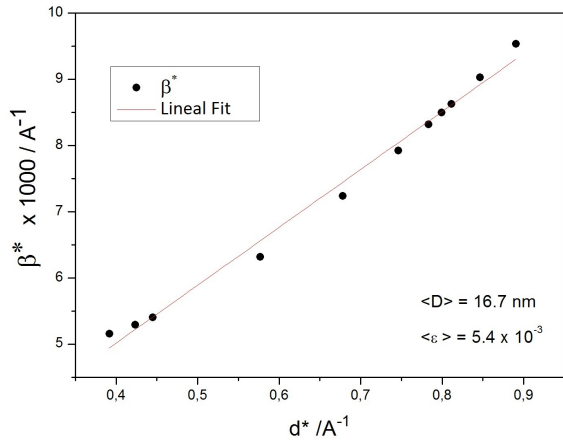


Figure 7. W-H curve (isotropic case), where the inverse of the intercept of the straight line with the ordinate returns $\langle D \rangle$ and the slope gives the average non-uniform microstrains value.

The average crystallite size is $\langle D \rangle = (16.7 \pm 0.2)$ nm and the non-uniform microstrains value is $\langle \epsilon \rangle = (16.7 \pm 0.2) \times 10^{-3}$. The result suggests that a decrease of Al content not only diminishes the probability of occurrence of planar defects but also leads to a decrease of $\langle D \rangle$ and an increase of $\langle \epsilon \rangle$ in the alloy. This result is in agreement with another report, in which a composition close to $x = 0.05$ was analyzed as well [8].

On the other hand, deformation defect density values have been also reported for compositions close to $x = 0.05$, and even in pure Ti (hcp) [8]. An empirical relationship between deformation defect density and Al content has been also proposed. However, as has already been mentioned, the methodology used within the WA method in this report could have led to these results. In this work, based on the qualitative analysis carried out in section 3.2 and taking into account the absence of reflections corresponding to an fcc-type sequence, it is not obvious to assume the long-range presence of this type of defect in the crystal structure of this composition.

Although the magnitudes $\langle D \rangle$ and $\langle \epsilon \rangle$ determined by the two methods are not strictly the same by definition, they allow an appropriate description of the evolution of the microstructure of the $\text{Al}_x\text{Ti}_{3-x}$ alloy.

V. CONCLUSIONS

Qualitative analysis shows the occurrence of a compositional order-disorder transition in aluminum-titanium alloys ($\text{Al}_x\text{Ti}_{3-x}$) within the composition range $0.05 \leq x \leq 0.20$, as well as the existence of a composition-dependent fcc phase embedded in the hcp matrix. This minority fcc phase indicates the presence of planar defects, decreasing its volume fraction

as a function of the Al content. The lattice parameters and the interplanar distance constitute order parameters of the phase transition.

The selection of the WA and WH methods for the microstructural characterization was carried out on the basis of the characteristics presented in the XRD patterns. The analysis allowed to establish that in this type of alloy (i) the occurrence of deformation defects predominates, while the growth is absent, (ii) the average crystallite size decreases, while nonuniform microstrains increase slightly when the system moves towards a higher concentration of Ti.

ACKNOWLEDGEMENTS

Dr. A. Pentón-Madrigal thanks CBPF Brazil for partial financial support in the framework of its graduate program. This work was also supported by a project associated to the National Program of Fundamental Science (MES-UH-2018 Cuba). Thanks also to Dr. A. Fundora for XRD experiments support.

REFERENCES

- [1] V.I. Fadeeva, A.V. Leonov, E. Szweczek, H. Matyja, *Mat. Sci. Engng.* **A242**, 230 (1998).
- [2] S.G. Lakshmi, D. Arivuoli, B. Ganguli, *Mater. Chem. Phys.* **76**, 187 (2002).
- [3] S. Diplas, P. Tsakirooulos, et al., *Acta Mater.* **8**, 1951 (2002).
- [4] X. D. Zhang, J. M. K. Wiezorek, M. J. Kaufman, M. H. Loretto and H. L. Fraser, *Phil. Mag.* **79**, 519 (1999)
- [5] P. Sahu, *Intermetallics* **14**, 180 (2006)
- [6] G. Karmaker, P. Mukherjee, et al., *Bull. Mater. Sci.* **24**, 649 (2001).
- [7] E. A. Metzbowyer, *Metallurgical Transactions* **2**, 3099 (1971).
- [8] J. Ghosh, S.K. Chattopadhyay, A.K. Meikap, S.K. Chatterjee. *J. Alloys Comp.* **453**, 131 (2008).
- [9] Warren B.E., *X-ray diffraction*, Addison-Wesley (1969).
- [10] Williamson G.K., Hall W.H., *Acta Met.* **1**, 22 (1953).
- [11] Massalski T. B. et al. *Binary alloy phase diagrams*. Vol. 1-3. Materials Park, Ohio, ASM International, (1990).
- [12] *U.P.B. Sci. Bull, series B* **68**, 4 (2006).
- [13] R. Croche, L. Gatineau, *J. Appl. Cryst.* **10**, 479 (1977).
- [14] D. Balzar, H. Ledbetter, *J. Appl. Cryst.*, **26**, 97 (1993).
- [15] B.E. Warren, B.L. Averbach, *J. Appl. Phys.* **21**, 595 (1950).
- [16] G. K. Willianson, R.E. Smallman, *Acta Cryst.* **7**, 574 (1954).
- [17] G. B. Mitra, N.C. Halder, *Acta Cryst.* **17**, 817 (1964).
- [18] Krumm SS. WINFIT 1.0. XIIIth Conf. Clay Mineralogy and Petrology, Prague1994. *Acta Univ. Carolinae Geol.* **38**, 253 (1994).
- [19] S. K. Gupta. *J. Appl. Cryst.* **31**, 476 (1998).
- [20] *Inorganic Crystal Structure Database (ICSD)*, versión 1.4.4, 2008.
- [21] D. B. Cullity, *Elementsof X-ray Diffraction*, Chapter 12, p.352. Addison & Wesley (1956).

- [22] Inertational Table for Crystallography, Vol. A: Space Group Symmetry. D. Reidel Publishing Company Dordrecht :Holland/ Boston, U.S.A. (1983).
- [23] A. Blandin, J. Friedel, G. Saada, J. Phys. **27**, 3 (1966).
- [24] G. Caglioti, A. Paoletti, F.P. Ricci, Nucl. Instrum. **3**, 233 (1958).
- [25] J. Rodríguez-Carvajal: FULLPROF: A Program for Rietveld Refinement and Pattern Matching Analysis, Abstracts of the Satellite Meeting on Power Diffraction of the XVth Congress International Union of Crystallography, Toulouse, France. (1990), p. 127.
- [26] H.M. Rietveld, J. Appl. Cryst. **2**, 65 (1969).
- [27] A. Le Bail, H. Duroy, J. L. Fourquet, Mater. Res. Bull. **23**, 447 (1988).

This work is licensed under the Creative Commons Attribution-NonCommercial 4.0 International (CC BY-NC 4.0, <http://creativecommons.org/licenses/by-nc/4.0>) license.

